Chemical Science

ROYAL SOCIETY OF CHEMISTRY

EDGE ARTICLE

View Article Online
View Journal | View Issue

Cite this: *Chem. Sci.*, 2022, **13**, 10752

All publication charges for this article have been paid for by the Royal Society of Chemistry

Received 7th July 2022
Accepted 27th July 2022

DOI: 10.1039/d2sc03783a

rsc.li/chemical-science

Multiple Pickering emulsions stabilized by surface-segregated micelles with adaptive wettability†

Tongtong Zhang,[a] Hang Jiang,[b] Liangzhi Hong *[ac] and To Ngai *[d]

Surface-segregated micelles (SSMs) with adaptive wettability have considerable potential for application in Pickering emulsions and bioanalytical technology. In this study, spherical SSMs were prepared *via* polymerization-induced self-assembly co-mediated with a binary mixture of macromolecular chain transfer agents: pH-responsive poly(2-(dimethylamino) ethyl methacrylate) and hydrophobic polydimethylsiloxane. Using these SSMs as the sole emulsifier, we adjusted the pH to successfully produce both water-in-oil-in-water (W/O/W) and oil-in-water-in-oil (O/W/O) multiple emulsions through a single-step emulsification process. Moreover, we demonstrated that multiple emulsion systems with adjustable pH are suitable for the development of an efficient and recyclable interfacial catalytic system. Multiple emulsion microreactors increase the area of the oil–water interface and are therefore more efficient than the commonly used O/W and W/O emulsion systems.

Introduction

Particle-stabilized emulsions, also known as Pickering emulsions, which have been largely ignored since they were first reported in early 1907, are recently receiving increasing academic attention.[1–3] The inherent advantages of Pickering emulsions—their excellent stability and surfactant-free characteristics—make them attractive for numerous applications relating to food,[4] pharmaceuticals,[5] crude oil recovery,[6] and catalysis.[7,8] The type and stability of a Pickering emulsion are closely related to the wettability of the colloidal particles. Generally, the main wetting liquid forms the continuous phase and the other liquid forms the dispersed phase.[9] Hydrophilic particles with contact angle < 90° are suitable for the stabilization of water-in-oil (O/W) emulsions, and hydrophobic particles with contact angle > 90° are more suitable for the stabilization of water-in-oil (W/O) emulsions. Particles that are completely wetted by water or oil are dispersed in this phase and cannot form an emulsion.[10] The wettability of particles can be tailored by modifying the surface chemistry and topology (*e.g.*, roughness).[11]

In general, multiple Pickering emulsions, also called "emulsions of emulsions," have been prepared through a two-step emulsification process using a binary mixture of particles differing in wettability.[1,12,13] Binks and colleagues prepared stable multiple emulsions containing ionic liquids stabilized by silica nanoparticles that differed in their SiOH content.[14] They also found that multiple Pickering emulsions could be prepared from a mixture of hydrophilic and hydrophobic pigments.[15] Armes and colleagues tuned the wettability of silica particles by coating them with poly(ethylene imine) and then enabling a subsequent reaction with 1-undecanal through Schiff base chemistry.[16,17] Fujii and colleagues demonstrated that the wettability of hydroxyapatite (HAp) particles could be tuned through the adsorption of poly(L-lactic acid) (PLLA) and that a stable multiple emulsion could be prepared using a combination of PLLA-coated HAp and pristine HAp particles.[18] Ning and colleagues produced water-in-oil-in-water (W/O/W) double Pickering emulsions with hydrophobic silica H30 and hydrophilic mesoporous silica nanoparticles.[19] They also prepared hierarchical porous polymeric microspheres and capsule clusters based on a double Pickering emulsion with a polymerizable middle oil phase.[20,21] Contact angle hysteresis of microbowls can be leveraged to prepare multiple Pickering emulsions by using a silicone microbowl as a sole stabilizer.[22] Sabri and colleagues demonstrated that highly viscous multiple Pickering emulsions could be prepared with a single type of silica nanoparticle grafted with silanes and sodium alginate.[23] We have previously reported the wetting properties of mixed polymer brush-coated nanoparticles prepared by grafting μ-poly (ethylene glycol)-*b*-polystyrene-*b*-poly [(3-triisopropoxysilyl) propyl methacrylate] (μ-PEG-*b*-PS-*b*-PIPSMA) miktoarm star polymers onto the surface of silica nanoparticles.[24] The

[a]*Faculty of Materials Science and Engineering, South China University of Technology, Guangzhou 510640, P. R. China. E-mail: mslzhong@scut.edu.cn*

[b]*The Key Laboratory of Synthetic and Biological Colloids, Ministry of Education & School of Chemical and Material Engineering, Jiangnan University, Wuxi 214122, P. R. China*

[c]*Guangdong Provincial Key Laboratory of Luminescence from Molecular Aggregates, South China University of Technology, Guangzhou 510640, P. R. China*

[d]*Department of Chemistry, The Chinese University of Hong Kong, Shatin N.T., Hong Kong, P. R. China. E-mail: tongai@cuhk.edu.hk*

† Electronic supplementary information (ESI) available. See https://doi.org/10.1039/d2sc03783a

wettability of the prepared nanoparticles depends on the initial dispersing phase. In addition, one-step formation of oil-in-water-in-oil (O/W/O) multiple emulsions was achieved with these hairy particles initially dispersed in both aqueous and oil phases. Recently, W/O/W high internal double emulsions with a combination of lecithin surfactant and silica particles were produced.[25]

Block nanoparticles produced by polymerization-induced self-assembly (PISA) have been used as emulsifiers to prepare Pickering emulsions.[26,27] Through PISA, a series of block copolymer nanoparticles in high concentration can be prepared.[28,29] The surface properties of nanoparticles can be tuned through judicious selection of the macromolecular chain transfer agents (macro-CTAs) for a given core-forming block,[30,31] which is likely to be of considerable interest in the design of new Pickering emulsifiers. Wang and colleagues reported that the cross-linked worms prepared by PISA could individually stabilize a Pickering high internal phase emulsion, which can then be used as a template for the fabrication of hybrid porous materials.[32] Yuan and colleagues demonstrated that the droplet size of an O/W Pickering emulsion could be regulated by adjusting the size of the block copolymer nanoparticles.[33] Armes and colleagues reported that multiple Pickering emulsions could be stabilized by a combination of hydrophilic and hydrophobic block copolymer worms through a two-step emulsification process.[34]

Surface-segregated micelles (SSMs) can be easily fabricated by reversible addition–fragmentation chain transfer (RAFT) dispersion polymerization mediated with a binary mixture of two macro-CTAs.[35,36] During the core-forming self-assembly process, the microphase separation between the two macro-CTAs simultaneously leads to the formation of discrete coronal nodules. Micelles with phase-segregated corona render the surface with switching and adaptive properties.[37] In this study, a binary mixture of hydrophobic polydimethylsiloxane (PDMS; D-CTA) and hydrophilic poly(2-(dimethylamino) ethyl methacrylate) (PDMAEMA; E-CTA) macro-CTAs were used for the dispersion polymerization of benzyl methacrylate (BzMA) in isopropanol. Isopropanol is a good solvent for E-CTA, a marginal solvent for D-CTA, and a poor solvent for poly(-benzyl methacrylate) (PBzMA). The preparation of multiple emulsions usually requires two types of wettable particle and a two-step emulsification process.[34] However, we found that SSMs with adaptive wettability could be used as the sole particle emulsifier to stabilize both W/O/W and O/W/O multiple emulsions. Furthermore, we demonstrated that these switchable multiple emulsions are suitable for the development of an efficient and recyclable interfacial catalytic system.

Results and discussion

Synthesis of SSMs

SSMs were synthesized by RAFT dispersion polymerization of benzyl methacrylate (BzMA) co-mediated with $PDMAEMA_{46}$ macro-CTA (E_{46}-CTA) and $PDMS_{60}$ macro-CTA (D_{60}-CTA), as shown in Scheme 1, wherein the subscript denotes the degree of polymerization (DP) of corresponding blocks. E_{46}-CTA was

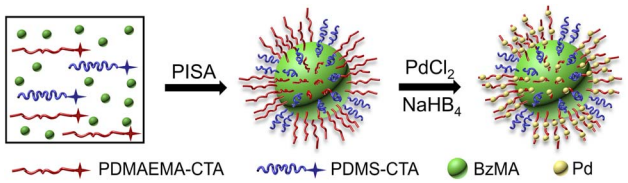

Scheme 1 Schematic showing synthesis of SSMs by RAFT dispersion polymerization induced self-assembly co-mediated with $PDMAEMA_{46}$ macro-CTA (E_{46}-CTA) and $PDMS_{60}$ macro-CTA (D_{60}-CTA), and the fabrication of palladium-coated SSMs.

synthesized by RAFT polymerization of DMAEMA in tetrahydrofuran (THF), using 4-cyanopentanoic acid dithiobenzoate (CPADB) as the chain transfer agent and azobisisobutyronitrile (AIBN) as the initiator.[38] D_{60}-CTA was prepared by dicyclohexylcarbodiimide/(dimethylamino)pyrimidine (DCC/DMAP)-catalyzed esterification of monocarbinol-terminated PDMS with CPADB.[39] The nanoparticles are composed of two diblock copolymers—PDMAEMA-*b*-PBzMA and PDMS-*b*-PBzMA—with PBzMA as the core and PDMS and PDMAEMA as the mixed coronas. For brevity, PDMS, PDMAEMA, and PBzMA are hereinafter referred to as D, E, and B, respectively.

As observed in Fig. 1a, after 30 h of reaction, the conversion of BzMA was 97.3% and the DP of PBzMA was 195. The diblock copolymer mixture is denoted as $[D_{60}/(E_{46})_4]$-B_{195}; the subscript denotes the DP of each block, calculated by ^{1}H nuclear magnetic

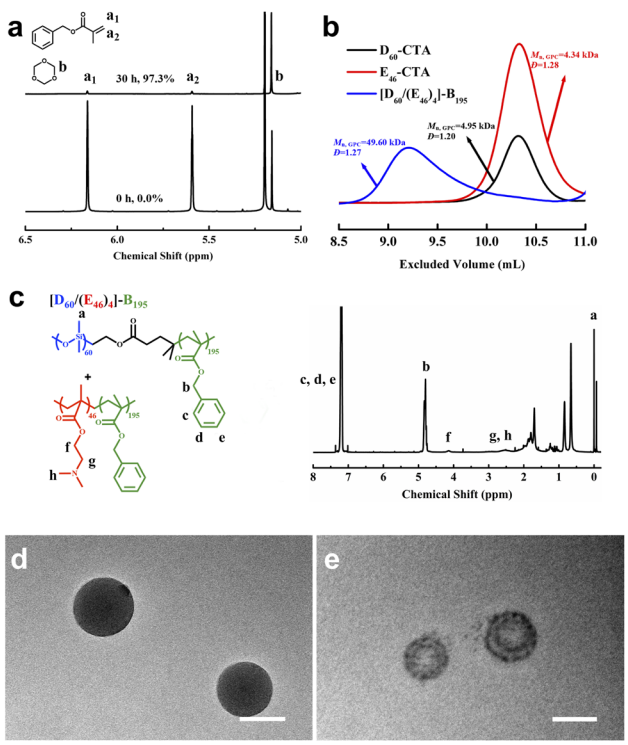

Fig. 1 (a) Comparison of ^{1}H NMR ($CDCl_3$) spectra at 0 and 30 h. (b) GPC traces. (c) ^{1}H NMR spectrum of $[D_{60}/(E_{46})_4]$-B_{195} diblock copolymer mixture in $CDCl_3$. (d and e) Transmission electron microscopy (TEM) images of $[D_{60}/(E_{46})_4]$-B_{195} nanoparticles without CH_3I staining (d) and with CH_3I staining (e) Scale bars indicate 100 nm.

resonance (NMR). The $[D_{60}/(E_{46})_4]$-B_{195} micellar aggregates were isolated by centrifugation, washed with isopropanol, and vacuum dried at room temperature for gel permeation chromatography (GPC) and ^{1}H NMR analyses. The GPC result (Fig. 1b) shows that the polydispersity index ($Đ$) of $[D_{60}/(E_{46})_4]$-B_{195} is 1.27. Fig. 1c shows the ^{1}H NMR spectra of $[D_{60}/(E_{46})_4]$-B_{195} in $CDCl_3$. The characteristic peak of PDMS is observed at around 0.1 ppm for the protons of the methyl group attached to silicon. The peaks in the range 7.27–7.34 ppm correspond to the protons of the phenyl group of BzMA. The peak corresponding to the methylene protons adjacent to the phenyl group in the PBzMA block is observed at 4.87 ppm (Fig. 1c). The range 2.28–3.19 ppm corresponds to the $N(CH_3)_2$ group and the CH_2 group adjacent to the $N(CH_3)_2$ group from PDMAEMA. The methylene protons adjacent to the backbone ester group in the PDMAEMA block are observed at 4.18 ppm (Fig. 1c). To further fix the SSMs structure, ethylene glycol dimethacrylate was added at the late stage of polymerization.[26]

Particle morphology and properties

The morphologies of the $[D_{60}/(E_{46})_4]$-B_{195} nanoparticles were investigated by transmission electronic microscopy (TEM) with and without CH_3I vapor staining (Fig. 1d and e). CH_3I vapor can selectively stain the tertiary amine groups of the PDMAEMA block. The unstained TEM image shows that the $[D_{60}/(E_{46})_4]$-B_{195} nanoparticles were spherical micelles with a diameter of 113 ± 14 nm (the standard deviation was calculated from the measurements of 60 particles). After CH_3I staining, the black nanodomain was the hydrophilic PDMAEMA microphase and the gray area was the hydrophobic PDMS microphase, demonstrating the successful preparation of the SSMs.

The size of the dispersed $[D_{60}/(E_{46})_4]$-B_{195} nanoparticles was determined through characterization by dynamic light scattering (DLS). The resulting nanoparticles had a mean hydrodynamic diameter of 141 ± 7 nm (Fig. S1†). The mean diameter obtained from the TEM image was smaller than that obtained through DLS; this difference may be attributed to the dryness of the TEM samples and an overestimation of the particle size through DLS, as stronger scattering of larger particles increases the overall particle size.[20,31,40]

E-CTA is a water-soluble polymer that is sensitive to pH and temperature.[41] We speculated that the corona chain segregation pattern of $[D_{60}/(E_{46})_4]$-B_{195} micellar aggregates, when used as particulate emulsifiers, might exhibit switchable or adaptive wettability. We first studied the effect of the concentration of $[D_{60}/(E_{46})_4]$-B_{195} nanoparticles on Pickering emulsions. The Pickering emulsions were prepared by homogenizing a mixture of toluene and deionized (DI) water at 15 000 rpm for 120 s with different emulsifier concentrations at pH = 2. As shown in Fig. S2,† as the concentration of micellar aggregates increased, the droplet size of the Pickering emulsion decreased. For emulsions with a higher concentration of nanoparticles, a larger number of polymeric nanoparticles could be used to cover the oil–water interface and then stabilize the emulsions. Thus, we obtained an O/W Pickering emulsion with a smaller droplet size. This concentration-dependent droplet size of an emulsion is a typical characteristic of particulate emulsifiers in Pickering emulsions.[33]

Preparation of pH-switchable multiple emulsions

As the PDMAEMA block is pH-responsive and has a pKa of 8.0,[42] the hydrophilic/hydrophobic properties of the block copolymer aggregates can be easily adjusted by changing the pH. Although Protat and colleagues reported a responsive emulsion stabilized by PDMAEMA-*b*-PDMS block copolymers,[43] it has been demonstrated that emulsions stabilized by micellar aggregates exhibited higher droplet stability.[44] The confocal laser scanning microscopy (CLSM) images shown in Fig. 2 illustrate how the pH of the aqueous phase affects the type of emulsion stabilized by the spherical $[D_{60}/(E_{46})_4]$-B_{195} micellar aggregates. To clearly demonstrate the emulsion type, the oil phase was dyed with Nile red. At pH = 5.0, stable O/W emulsions were obtained, as verified by the confocal images in Fig. 2e. At pH = 7.0, W/O/W multiple emulsions were obtained (Fig. 2f). Notably, at pH = 9.0, O/W/O multiple emulsions were obtained through a one-step emulsification process (Fig. 2g). When the pH was increased to 12.0, the emulsion type transformed to W/O, as show in Fig. 2h. Multiple emulsions are typically prepared through a two-step emulsification process using two types of particles.[34] We previously reported that multiple emulsions could be prepared through a one-step emulsification process using environmentally responsive silica particles as the sole stabilizer.[24] However, only O/W/O emulsions were obtained through that method. In this study, both W/O/W and O/W/O

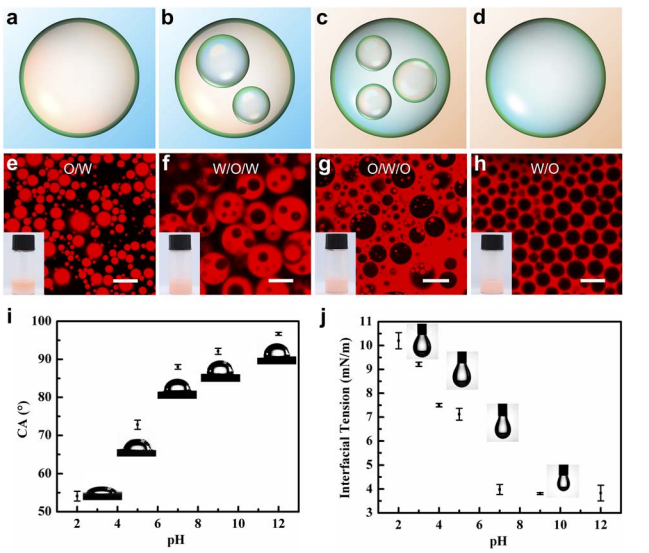

Fig. 2 (a–d) Illustration of emulsion types at pH = 5.0, 7.0, 9.0, and 12.0, respectively. (e–h) CLSM images of stabilized emulsions prepared at different pH: pH = 5.0 (e), pH = 7.0 (f), pH = 9.0 (g), and pH = 12.0 (h). The concentration of $[D_{60}/(E_{46})_4]$-B_{195} is 0.15 wt% of the total mass of oil and water. The oil phase is toluene and is dyed with Nile red. The scale bars in all images are 30 μm. (i) Three-phase contact angles (θ_{ow}) of the $[D_{60}/(E_{46})_4]$-B_{195} nanoparticles at different pH values. (j) The equilibrium interfacial tension between oil and water at different pH. $[D_{60}/(E_{46})_4]$-B_{195} nanoparticles were used as surfactant; the concentration of $[D_{60}/(E_{46})_4]$-B_{195} in toluene is 2.8 mg mL^{-1}.

multiple emulsions were obtained by tuning the pH of the aqueous phase. As multiple emulsions have considerable potential in the pharmaceutical, cosmetics, and food industries, microphase-segregated mixed micelles are innovative particle stabilizers for the preparation of tunable multiple emulsions.

Interfacial wettability is a key parameter in the preparation of particle-stabilized emulsions. The wettability of particles is closely related to three-phase contact angles (θ_{ow}). The θ_{ow} of the $[D_{60}/(E_{46})_4]$-B_{195} micellar nanoparticles was measured using the classical drop shape method.[45,46] Fig. 2i shows images of water droplets on the $[D_{60}/(E_{46})_4]$-B_{195} tablets in toluene. When pH < 8, the contact angle was less than 90°; when pH > 8, the contact angle was greater than 90°. This behavior is attributable to the pH-sensitive PDMAEMA polymer, which can be protonated under acidic conditions and deprotonated under alkaline conditions. The protonated PDMAEMA chain is more hydrophilic than the deprotonated chain. When θ_{ow} < 90°, the $[D_{60}/(E_{46})_4]$-B_{195} nanoparticles are relatively hydrophilic and generally produce an emulsion with water as the continuous phase. When θ_{ow} > 90°, the micellar nanoparticles are relatively hydrophobic, potentially promoting the formation of an emulsion with oil as the continuous phase. When θ_{ow} is close to 90°, the nanoparticles can stabilize both oil droplets and water droplets, thus enabling the preparation of multiple emulsions. When the contact angle is close to but less than 90°, the type of emulsion produced is W/O/W. When the contact angle is close to but greater than 90°, the type of emulsion produced is O/W/O.

Fig. 2j shows the effect of the pH of the aqueous phase on the interfacial tension (IFT) between oil and water with $[D_{60}/(E_{46})_4]$-B_{195} nanoparticles as emulsifiers. In the presence of $[D_{60}/(E_{46})_4]$-B_{195} micelles, IFT considerably decreased. As the pH value increased, IFT decreased and eventually reached a constant value. The hydrodynamic radius (R_h) of the copolymer mixture micelles was measured at various pH values of the solution. As depicted in Fig. S3,† when the pH was increased from 2 to 12, R_h of the $[D_{60}/(E_{46})_4]$-B_{195} micelles gradually decreased from 241.2 to 200.2 nm; this decrease is attributable to the deswelling of micellar corona caused by the deprotonation of dimethylamino groups as the pH value increased. The zeta potentials (ζ) of $[D_{60}/(E_{46})_4]$-B_{195} micelles at different pH values are shown in Fig. S3.† As evident, the zeta potential of the nanoparticles ranged from 33.9 to −46.3 mV under the measured pH conditions. The variation in the zeta potential may be attributable to the protonation and deprotonation of the PDMAEMA segment in the $[D_{60}/(E_{46})_4]$-B_{195} copolymer mixture. Under acidic conditions, a high degree of protonation resulted in positively charged micellar corona with a high zeta potential. In contrast, under neutral or alkaline conditions, deprotonation resulted in negative zeta potential.

Loading of Pd nanoparticles on colloidal particles

Such a pH-switchable multiple emulsion may be suitable for the development of an efficient and recyclable interfacial catalytic system.[47] The performance of an interfacial catalytic system is considerably affected by the interfacial area and the mass transportation rate of reactants. We envision that compared with the O/W or W/O Pickering interfacial catalytic systems reported in previous studies,[48,49] multiple Pickering emulsions may further enhance catalytic efficiency by increasing the interfacial area and decreasing the diffusion distance. As a proof of concept, we prepared $[D_{60}/(E_{46})_4]$-B_{195}-supported palladium nanoparticles (Pd/$[D_{60}/(E_{46})_4]$-B_{195}) through *in situ* growing of Pd nanoparticles onto the PDMAEMA domain and then investigated the effect of the emulsion type on the interfacial catalytic efficiency of Pd/$[D_{60}/(E_{46})_4]$-B_{195}. Fig. 3a shows the typical TEM image of Pd/$[D_{60}/(E_{46})_4]$-B_{195}. TEM energy-dispersive X-ray spectroscopy (EDX) mapping of Pd/$[D_{60}/(E_{46})_4]$-B_{195} further confirmed that Pd nanoparticles with a diameter of 4.1 ± 1.0 nm (yellow dot in Fig. 3b) were successfully distributed on the surface of Pd/$[D_{60}/(E_{46})_4]$-B_{195}.

Notably, after being loaded with Pd nanoparticles, the Pd/$[D_{60}/(E_{46})_4]$-B_{195} colloidal nanocomposite continued to possess the ability to stabilize multiple emulsions in response to change in the pH. At pH = 6.0, O/W emulsions were obtained (Fig. 3d), and at pH = 7.0, W/O/W multiple emulsions were obtained (Fig. 3e). When the pH was increased to 9.0, O/W/O multiple emulsions were obtained (Fig. 3f). A further increase in the pH to 10.0 resulted in a typical phase inversion, and the toluene in the formed emulsion was the continuous phase; thus, W/O emulsion was obtained (Fig. 3g). Compared with $[D_{60}/(E_{46})_4]$-B_{195} micellar aggregates, Pd/$[D_{60}/(E_{46})_4]$-B_{195}-stabilized emulsions continued to be pH-responsive. Noting that non-spherial multiple emulsion droplets are formed when the SSMs are loaded with Pd (Fig. 3e and f). When the mixed micelles are loaded with Pd nanoparticles, the initial positive zeta potential decrease due to the negatively charged Pd nanoparticles. We speculated that such change of surface charge induced the interfacial jamming of micelle hybrid nanoparticles at oil-water interfaces, and then formed the non-spherical emulsion droplets.[50–53] Furthermore, the stability of Pickering emulsions stabilized by $[D_{60}/(E_{46})_4]$-B_{195} and Pd/$[D_{60}/(E_{46})_4]$-B_{195} nanoparticles were studied; the results are shown in Fig. S4 and S5.† The confocal microscopy images of the emulsions stabilized by $[D_{60}/(E_{46})_4]$-B_{195} and Pd/$[D_{60}/(E_{46})_4]$-B_{195} nanoparticles showed

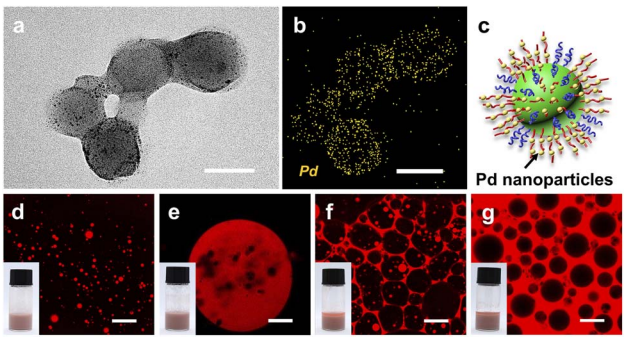

Fig. 3 (a) TEM images for Pd/$[D_{60}/(E_{46})_4]$-B_{195}-supported palladium nanoparticles. (b) Elemental mapping of Pd. (c) Illustration of Pd/$[D_{60}/(E_{46})_4]$-B_{195}. (d–g) CLSM images of the emulsions stabilized by Pd/$[D_{60}/(E_{46})_4]$-B_{195} at different pH: pH = 6.0 (d), pH = 7.0 (e), pH = 9.0 (f), and pH = 10.0 (g). The oil phase is toluene and is dyed with Nile red. Scale bars in (a) and (b) show 100 nm, and those in (d)–(g) show 30 μm.

that the emulsion type remained unchanged after 30 days of storage.

Evaluation of catalysis efficiency

Next, the catalysis efficiency of Pd/$[D_{60}/(E_{46})_4]$-B_{195}-stabilized Pickering emulsion microreactors was examined *via* the hydrogenation of *p*-nitroanisole in the presence of $NaBH_4$. Toluene containing *p*-nitroanisole and Pd/$[D_{60}/(E_{46})_4]$-B_{195} was emulsified with water; then, an aqueous solution of $NaBH_4$ was added into the emulsion and gently stirred. As shown in Fig. 4a, the emulsion type did not change before and after the catalytic hydrogenation reaction. During the biphasic catalysis reaction, $NaBH_4$ in the aqueous phase was used as the source of hydrogen for the reduction of the nitro groups; meanwhile, *p*-nitroanisole from the toluene phase adhered to the surface of Pd/$[D_{60}/(E_{46})_4]$-B_{195}. As a result, the adsorbed hydrogen transferred to the nitro groups on the oil–water interfaces (Fig. 4b). After 6 h of reaction, the oil phase could be separated by centrifugation followed by simple decantation. The yields were calculated by ^{1}H NMR, as shown in Fig. S6.† We then evaluated the effect of the emulsion type on the catalytic efficiency of these emulsion systems, as shown in Fig. 4c. At pH = 6.0, O/W Pickering emulsion microreactors achieved 85% conversion of *p*-nitroanisole. Notably, the conversion obtained at pH = 7.0 with W/O/W multiple emulsions was even higher than that with O/W emulsion systems. We speculate that the multiple emulsion system increases the area of the oil–water interface (Fig. S8†). Similarly, O/W/O multiple emulsion microreactors also achieved a high conversion of *p*-nitroanisole. However, at pH = 10.0, W/O emulsion reactors achieved a lower conversion of *p*-nitroanisole. As shown in Fig. 4a, the size of the droplets of the W/O emulsion was larger than that of the droplets of the O/W emulsion. In contrast, without emulsification, the conversion of *p*-nitroanisole was much lower than that of these emulsion systems. For the interfacial reduction of *p*-nitroanisole, the pH of aqueous phase will affect the catalysis efficiency through tuning the hydrophobicity of the particle stabilizer, because *p*-nitroanisole is easily absorbed on the hydrophobic surface.[54] High pH renders the Pd/$[D_{60}/(E_{46})_4]$-B_{195} surface more hydrophobic, suggesting that the catalytic efficiency can be improved at high pH by absorbing more *p*-nitroanisole on the surface. However, as shown in Fig. 4, the pH of aqueous solution also affects the emulsion type of the Pd/$[D_{60}/(E_{46})_4]$-B_{195} stabilized Pickering emulsion owing to the pH-responsive of PDMAEMA block. When the pH is 7.0 and 9.0, W/O/W and O/W/O were prepared, respectively. We found that multiple emulsion microreactors are more efficient than the commonly used O/W and W/O emulsion systems. These results indicates that although pH has an effect on the catalytic efficiency, the enlargement of interfacial area and the reduction of diffusion distance play a dominant role in the improvement of the interfacial catalytic efficiency.

Furthermore, we found that these multiple Pickering emulsion catalysis systems could be recycled and reused many times while maintaining high catalytic efficiency. For a subsequent reaction cycle, fresh solvent and substrate were added into the residual water phase. A W/O/W Pickering emulsion stabilized by Pd/$[D_{60}/(E_{46})_4]$-B_{195} nanoparticles was obtained again after adjustment of the pH to 7.0 and homogenization. The other processes in the reaction and catalyst recycling remained the same as in the first reaction cycle. As shown in Fig. S7,† from the first cycle to the fifth cycle, all of the *p*-anisidine yields were greater than 96%. The high catalytic efficiency and excellent recyclability indicate that the multiple Pickering emulsion stabilized by SSMs is a highly efficient interfacial catalysis strategy.

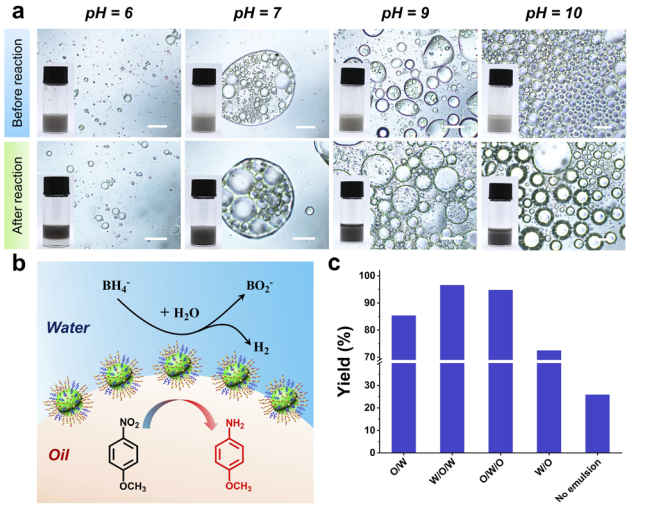

Fig. 4 Interfacial reduction of *p*-nitroanisole catalyzed by Pd/$[D_{60}/(E_{46})_4]$-B_{195}. (a) Optical microscope images of Pickering emulsions before and after reactions at different pH. (b) Catalytic mechanism of the interfacial reduction of *p*-nitroanisole with Pd/$[D_{60}/(E_{46})_4]$-B_{195}. (c) Conversion of *p*-nitroanisole dissolved in toluene in contact with water of different pH at 25 °C for 360 min. The scale bars in all images are 30 μm.

Conclusion

We demonstrated that surface-segregated micelles could be easily prepared by PISA co-mediated with a binary mixture of macro-CTAs. The surface-segregated structure has adaptive wettability. With spherical $[D_{60}/(E_{46})_4]$-B_{195} mixture micelles as the sole particulate emulsifier, O/W, W/O/W, O/W/O, and W/O emulsions can be obtained through a one-step emulsion process by adjusting the pH. To the best of our knowledge, the preparation of both W/O/W and O/W/O multiple emulsions using a sole particle stabilizer through a one-step emulsification process has not been previously reported. Furthermore, we illustrated that pH-switchable multiple emulsion systems are suitable for the development of an efficient and recyclable interfacial catalytic system. Multiple emulsion microreactors increase the area of the oil–water interface and are therefore more efficient than the commonly used O/W and W/O emulsion systems. By varying the ratio of E-CTA and D-CTA, the size of the microphase-separated nanodomain can be readily modulated. When the degree of polymerization of core-forming block BzMA increase, the morphology of micelles will change from sphere to worm, and then to vesicles.[55] These suggest that surface-

segregated micelles are versatile platforms for stabilizing complex liquid/liquid interfaces.

Data availability

All experimental supporting data and procedures are available in the ESI.†

Author contributions

L. H. and T. N. conceived and supervised the study; T. Z. performed experiments and data analysis; L. H., T. N. and H. J. reviewed the results and provided technical guidelines; all authors wrote the manuscript.

Conflicts of interest

There are no conflicts to declare.

Acknowledgements

This work is supported by the National Natural Science Foundation of China (Grant 21774035, 21374031); Science and Technology Planning Project of Guangdong Province, China (International Scientific Cooperation: 2020A0505100005); Key Laborotory of Polymeric Composite and Functional Materials of Ministry of Education (PCFM-2022A05); the Guangdong Provincial Key Laboratory of Luminescence from Molecular Aggregates, China (2019B030301003); and the Hong Kong Special Administration Region (HKSAR) General Research Fund (CUHK14304619, 2130642).

Notes and references

1 R. Aveyard, B. P. Binks and J. H. Clint, *Adv. Colloid Interface Sci.*, 2003, **100–102**, 503–546.
2 B. P. Binks, *Curr. Opin. Colloid Interface Sci.*, 2002, **7**, 21–41.
3 H. Jiang, Y. Sheng and T. Ngai, *Curr. Opin. Colloid Interface Sci.*, 2020, **49**, 1–15.
4 C. C. Berton-Carabin and K. Schroen, *Annu. Rev. Food Sci. Technol.*, 2015, **6**, 263–297.
5 J. Wu and G. H. Ma, *Small*, 2016, **12**, 4633–4648.
6 H. A. Son, K. Y. Yoon, G. J. Lee, J. W. Cho, S. K. Choi, J. W. Kim, K. C. Im, H. T. Kim, K. S. Lee and W. M. Sung, *J. Pet. Sci. Eng.*, 2015, **126**, 152–161.
7 W. J. Zhou, L. Fang, Z. Fan, B. Albela, L. Bonneviot, F. De Campo, M. Pera-Titus and J. M. Clacens, *J. Am. Chem. Soc.*, 2014, **136**, 4869–4872.
8 M. Pera-Titus, L. Leclercq, J. M. Clacens, F. De Campo and V. Nardello-Rataj, *Angew. Chem., Int. Ed.*, 2015, **54**, 2006–2021.
9 D. G. Ortiz, C. Pochat-Bohatier, J. Cambedouzou, M. Bechelany and P. Miele, *Engineering*, 2020, **6**, 468–482.
10 S. Levine, B. D. Bowen and S. J. Partridge, *Colloids Surf.*, 1989, **38**, 325–343.
11 M. Xiao, A. Xu, T. Zhang and L. Hong, *Front. Chem.*, 2018, **6**, 225.
12 L. Hong, G. Sun, J. Cai and T. Ngai, *Langmuir*, 2012, **28**, 2332–2336.
13 G. Sun, M. Liu, X. Zhou, L. Hong and T. Ngai, *Colloids Surf. A*, 2014, **454**, 16–22.
14 B. P. Binks, A. K. F. Dyab and P. D. I. Fletcher, *Chem. Commun.*, 2003, 2540–2541.
15 S. O. Olusanya and B. P. Binks, *J. Dispers. Sci. Technol.*, 2020, **43**, 1291–1304.
16 M. Williams, N. J. Warren, L. A. Fielding, S. P. Armes, P. Verstraete and J. Smets, *ACS Appl. Mater. Interfaces*, 2014, **6**, 20919–20927.
17 M. Williams, S. P. Armes, P. Verstraete and J. Smets, *Langmuir*, 2014, **30**, 2703–2711.
18 H. Maeda, M. Okada, S. Fujii, Y. Nakamura and T. Furuzono, *Langmuir*, 2010, **26**, 13727–13731.
19 Y. Ning, C. Wang, T. Ngai and Z. Tong, *Langmuir*, 2013, **29**, 5138–5144.
20 Y. Yang, C. Wang and Z. Tong, *RSC Adv.*, 2013, **3**, 4514–4517.
21 Y. Ning, Y. Yang, C. Wang, T. Ngai and Z. Tong, *Chem. Commun.*, 2013, **49**, 8761–8763.
22 Y. Nonomura, N. Kobayashi and N. Nakagawa, *Langmuir*, 2011, **27**, 4557–4562.
23 Y. Zhu, J. Sun, C. Yi, W. Wei and X. Liu, *Soft Matter*, 2016, **12**, 7577–7584.
24 M. Liu, X. Chen, Z. Yang, Z. Xu, L. Hong and T. Ngai, *ACS Appl. Mater. Interfaces*, 2016, **8**, 32250–32258.
25 X. Guan and T. Ngai, *Langmuir*, 2021, **37**, 2843–2854.
26 K. L. Thompson, P. Chambon, R. Verber and S. P. Armes, *J. Am. Chem. Soc.*, 2012, **134**, 12450–12453.
27 K. L. Thompson, C. J. Mable, A. Cockram, N. J. Warren, V. J. Cunningham, E. R. Jones, R. Verber and S. P. Armes, *Soft Matter*, 2014, **10**, 8615–8626.
28 X. Zhang, S. Boissé, W. Zhang, P. Beaunier, F. D'Agosto, J. Rieger and B. Charleux, *Macromolecules*, 2011, **44**, 4149–4158.
29 S. Boissé, J. Rieger, K. Belal, A. Di-Cicco, P. Beaunier, M. H. Li and B. Charleux, *Chem. Commun.*, 2010, **46**, 1950–1952.
30 M. Semsarilar, V. Ladmiral, A. Blanazs and S. P. Armes, *Langmuir*, 2012, **28**, 914–922.
31 C. Grazon, J. Rieger, N. Sanson and B. Charleux, *Soft Matter*, 2011, **7**, 3482–3490.
32 Q. Zhang, C. Wang, M. Fu, J. Wang and S. Zhu, *Polym. Chem.*, 2017, **8**, 5474–5480.
33 M. Zeng, X. Li, Y. Zhang, X. Chen, X. Sui and J. Yuan, *Polymer*, 2020, **206**, 122853.
34 K. L. Thompson, C. J. Mable, J. A. Lane, M. J. Derry, L. A. Fielding and S. P. Armes, *Langmuir*, 2015, **31**, 4137–4144.
35 S. Li, X. He, Q. Li, P. Shi and W. Zhang, *ACS Macro Lett.*, 2014, **3**, 916–921.
36 L. Sun, L. Hong and C. Wang, *Macromol. Rapid Commun.*, 2016, **37**, 691–699.
37 I. Luzinov, S. Minko and V. V. Tsukruk, *Soft Matter*, 2008, **4**, 714–725.
38 Y. Pei and A. B. Lowe, *Polym. Chem.*, 2014, **5**, 2342–2351.
39 A. P. Lopez-Oliva, N. J. Warren, A. Rajkumar, O. O. Mykhaylyk, M. J. Derry, K. E. B. Doncom,

M. J. Rymaruk and S. P. Armes, *Macromolecules*, 2015, **48**, 3547–3555.
40 F. Liu, J. Hu, G. Liu, S. Lin, Y. Tu, C. Hou, H. Zou, Y. Yang, Y. Wu and Y. Mo, *Polym. Chem.*, 2014, **5**, 1381–1392.
41 D. Fournier, R. Hoogenboom, H. M. L. Thijs, R. M. Paulus and U. S. Schubert, *Macromolecules*, 2007, **40**, 915–920.
42 D. Roy, J. S. Knapp, J. T. Guthrie and S. Perrier, *Biomacromolecules*, 2008, **9**, 91–99.
43 M. Protat, N. Bodin, F. Gobeaux, F. Malloggi, J. Daillant, N. Pantoustier, P. Guenoun and P. Perrin, *Langmuir*, 2016, **32**, 10912–10919.
44 S. J. Hunter and S. P. Armes, *Langmuir*, 2020, **36**, 15463–15484.
45 L. L. Dai, R. Sharma and C. Wu, *Langmuir*, 2005, **21**, 2641–2643.
46 C. Wu, S. Tarimala and L. L. Dai, *Langmuir*, 2006, **22**, 2112–2116.
47 H. Yang, T. Zhou and W. Zhang, *Angew. Chem., Int. Ed.*, 2013, **52**, 7455–7459.
48 H. Jiang, Y. Li, L. Hong and T. Ngai, *Chem.–Asian J.*, 2018, **13**, 3533–3539.
49 Y. Xi, B. Liu, H. Jiang, S. Yin, T. Ngai and X. Yang, *Chem. Sci.*, 2020, **11**, 3797–3803.
50 A. B. Subramaniam, M. Abkarian, L. Mahadevan and H. A. Stone, *Nature*, 2005, **438**, 930.
51 J. H. Luo, M. X. Zeng, B. L. Peng, Y. J. Tang, L. C. Zhang, P. M. Wang, L. P. He, D. L. Huang, L. Wang, X. Z. Wang, M. F. Chen, S. J. Lei, P. C. Lin, Y. Chen and Z. D. Cheng, *Angew. Chem., Int. Ed.*, 2018, **57**, 11752–11757.
52 J. W. Kim, D. Lee, H. C. Shum and D. A. Weitz, *Adv. Mater.*, 2008, **20**, 3239–3243.
53 M. M. Cui, T. Emrick and T. P. Russell, *Science*, 2013, **342**, 460–463.
54 L. Qi, Z. Luo and X. Lu, *Green Chem.*, 2018, **20**, 1538–1550.
55 T. Zhang, C. Zhan, X. Huang, Y. Huang, L. Zong, L. Hong and T. Ngai, *Macromol. Chem. Phys.*, 2021, **222**, 2100128.